

Analysis of the creep and dilatant behavior of a salt cavern in long-term using Brazilian geotechnical properties

Renathielli Fernanda da Silva Brunetta^{1#} , Alessander C. M. Kormann¹ ,

José Eduardo Gubaua² , Jucélio Tomás Pereira² 

Article

Keywords

Solution mining
Evaporitic rocks
Abaqus
Salt cavern abandonment
Finite element method
Nonlinear model

Abstract

The geomechanical behavior of a salt rock cavern was studied using Brazilian geotechnical properties. To design the finite element model, it was necessary to implement, using Fortran language, a constitutive model representing the creep behavior, since the model used is not native to the program. The constitutive model implemented was the Multiple Deformation Mechanism Model. This model was chosen for being a robust model that represents the primary and secondary phases of creep and presents good agreement with the Brazilian salt rocks. The analyzes considered a period of 50 years after the mine closure and five internal pressures acting in the analyzed cave. The pressures considered correspond to 40%, 50%, 60%, 70% and 80% of the vertical stress at the top of the mine. The creep and dilation behaviors were analyzed, and the creep deformations obtained in the simulations was acceptable in relation to the failure criterion adopted in this paper. However, only the design of experiment that considered the two biggest internal pressure resulted in a permissible micro-crack ratio value.

1. Introduction

Due to the products in its chain, chlorine and caustic soda are very relevant for society. Examples include polyvinyl chloride (PVC), agrochemicals, products for water and sewage treatment, pharmaceutical inputs, and lubricants (Jörissen, 2014).

Chlorine-soda is obtained by the electrolysis of a solution of rock salt (halite) in water. One of the rock salt mining techniques is dissolution extraction using recovery wells. The wells must reach the depth of saline material that can reach thousands of meters below the earth's surface. Afterwards, water is injected by these wells and when it comes into contact with rock salt, it dissolves the rock. Thus, it is possible to extract the brine used to obtain chlorine-soda. Curi (2017) presents a more detailed explanation about the extraction process.

Inevitably, at some point, the chlorine-soda extraction ceases. The most common technique of abandonment is to fill the cavern with brine and seal the well permanently. Thus, the pressure applied by the brine maintains the structural integrity of the cavern (Crotogino & Kepplinger, 2006). However, failures in the well seal, leakage through micro-cracks in the walls of the cave, tectonic movements,

and other factors, can cause loss of internal pressure in the cavern. Recent researches have been studied the possibility of using abandoned caverns for the storage of hydrocarbons (Thoraval et al., 2015; Wei et al., 2016a, b; Zhang et al., 2020a, b).

The study of cave abandonment involves three important aspects. The first aspect is the experimental characterization of the saline material. The second aspect is in-situ tests to investigate mine geometry. The third aspect is the applying constitutive models to simulate the material behavior. These models can predict the time-dependent behavior of the material (Thoraval et al., 2015).

Some evaporitic rocks, especially halite, have a very particular behavior. The material suffers permanent deformations under constant loads and/or high temperatures. These deformations change throughout time. This time-dependent behavior is known as creep (Costa, 1984). In the case of caverns, built on salt rocks, the material that surrounds the cavern flows into the cavern. This causes mass movement that reduces the cavern volume. As consequence, the mass movement can cause lowering of the terrain surface (subsidence). Subsidence and instabilities in salt-caverns regions are old geotechnical problems and found in several countries (Bell et al., 2000; Autin, 2002; Whyatt & Varley,


[#]Corresponding author. E-mail address: renathielli@hotmail.com

¹Universidade Federal do Paraná, Departamento de Construção Civil, Curitiba, PR, Brasil.

²Universidade Federal do Paraná, Laboratório de Mecânica dos Sólidos Computacional, Curitiba, PR, Brasil.

Submitted on June 23, 2022; Final Acceptance on March 19, 2023; Discussion open until December 30, 2023.

<https://doi.org/10.28927/SR.2023.006722>

 This is an Open Access article distributed under the terms of the Creative Commons Attribution License, which permits unrestricted use, distribution, and reproduction in any medium, provided the original work is properly cited.

2008; Yerro et al., 2014; Wang et al., 2018; Vassileva et al., 2021).

Creep occurs in three stages. The primary creep is where the strain rate decreases. The secondary creep follows the primary phase, with a constant strain rate. Finally, the tertiary phase. Literature does not characterize this phase well. But, in this phase, there may be an acceleration of the strain rate followed by the material rupture (Poiate Junior, 2012).

The dilatancy behavior of the saline rock is very important. A high level of stress can cause the generation of micro-cracks (Firme et al., 2019). Two domains define the salt rocks behavior. The first domain is compression. Here, the micro-cracks heal and guarantee the material impermeability. The second domain is dilatancy. The salt rock enters this domain when the active deviatoric stress exceeds the limit deviatoric stress. In this case, the expansion of the material can increase the permeability of the material (due to the occurrence of micro-cracks) and even cause damage (Van Sambeek et al., 1993).

Both dilatancy and creep behaviors can cause instabilities in abandoned caverns. This can lead to instabilities on the ground surface, such as subsidence. Although it is difficult to control the variables of a mine-abandonment project, due to its depth (it can be thousands of meters), maintaining an adequate internal pressure can help to avoid geotechnical instability. Therefore, the objective of this paper is to analyze the influence of internal pressure on the creep and dilation behavior of a rock salt mine with a geometry similar to those existing in the chlorine-soda mining fields in Brazil.

2. Constitutive modeling of rock salt

The constitutive relation applied to describe the rock salt behavior follows the Multiple Deformation Mechanism developed by Munson & Dawson (1979). The Multiple Deformation Mechanism allows simulating the creep behavior of rock salt under deviatoric stress. This model simulates transient (primary) and steady-state (secondary) creep phases. Different factors such as stress state, temperature, and material chemical composition, influence dislocations in salt rock (Firme et al., 2016). The Multiple Deformation Mechanism model uses three mechanisms to determine the steady-state phase creep: dislocation climb, undefined mechanism, and dislocation glide. The sum of them quantifies the secondary creep rate.

The dislocation climb can be described as a mechanism of thermal activation that depends on the stress intensity. This mechanism has a meaningful significance at high temperatures (approximately 50 °C). The high deformation energy generated during the dislocations leads to plastic deformation and hardening. The climb mechanism allows the movement of the dislocations (Firme et al., 2016).

An Arrhenius expression determines the contribution of dislocation climb on steady-state creep rate ($\dot{\epsilon}_{DC}$) as:

$$\dot{\epsilon}_{DC} = A_1 \left(\frac{\sigma_{eq}}{G} \right)^{n_1} \exp\left(\frac{-Q_1}{RT}\right) \quad (1)$$

In rocks, such as halite, the contribution of the dislocation climb is considerable when the temperature is above 40% of the melting temperature of the material. The second mechanism is known as undefined mechanism and its rate ($\dot{\epsilon}_{UM}$) is determined using an Arrhenius expression as the one used to determine the dislocation climb, defined as:

$$\dot{\epsilon}_{UM} = A_2 \left(\frac{\sigma_{eq}}{G} \right)^{n_2} \exp\left(\frac{-Q_2}{RT}\right) \quad (2)$$

The third mechanism used is the dislocation glide (*DGL*). It is a slow creep mechanism and arises from displacements in the material crystal lattice. This mechanism occurs at any stress level unbalanced by deviatoric stress. Shear stress also can influence the occurrence of this mechanism. Consequently, there is plastic strain and material hardening. The rate of this mechanism ($\dot{\epsilon}_{DG}$) is computed as:

$$\dot{\epsilon}_{DG} = \left| H(\sigma_{eq} - \sigma_0) \right| \times \left(B_1 \exp\left(\frac{-Q_1}{RT}\right) + B_2 \exp\left(\frac{-Q_2}{RT}\right) \right) \times \sinh\left(\frac{q(\sigma_{eq} - \sigma_0)}{G}\right) \quad (3)$$

In this equation, $\left| H(\sigma_{eq} - \sigma_0) \right|$ is a Heaviside step function with argument $(\sigma_{eq} - \sigma_0)$. This argument limits the occurrence of *DGL* for a deviatoric (or equivalent) stress higher than the reference stress value of the mechanism (σ_0).

The primary creep was determined by performing a retro analysis with the secondary creep rate. Thus, it is possible to estimate a limit strain during the transient creep (ϵ_t^*) as:

$$\epsilon_t^* = K_0 \exp^{cT} \left(\frac{\sigma_{eq}}{G} \right)^m \quad (4)$$

From (ϵ_t^*) it is possible to determine the function F as:

$$F = \begin{cases} \exp\left[\Delta\left(-\frac{\zeta}{\epsilon_t^*}\right)^2\right] & \text{if } \zeta < \epsilon_t^* \\ 1 & \text{if } \zeta = \epsilon_t^* \\ \exp\left[-\delta\left(-\frac{\zeta}{\epsilon_t^*}\right)^2\right] & \text{if } \zeta > \epsilon_t^* \end{cases} \quad (5)$$

In this equation, ζ is an internal isotropic hardening variable subject to an evolutionary rate ($\dot{\zeta}$) defined as:

$$\dot{\zeta} = (F -) \dot{\epsilon}_{SS} \quad (6)$$

The value of $\dot{\epsilon}_{SS}$ is obtained by the summation of the three micromechanical creep mechanisms presented in Equations 1, 2, and 3.

The hardening (Δ) and softening (δ) parameters are computed using:

$$\Delta = \alpha_h + \beta_h \log\left(\frac{\sigma_{eq}}{G}\right) \quad (7)$$

and

$$\delta = \alpha_s + \beta_s \log\left(\frac{\sigma_{eq}}{G}\right) \quad (8)$$

respectively.

Finally, the total creep rate ($\dot{\epsilon}$) is determine, including the primary and secondary creeps, by using:

$$\dot{\epsilon} = F \dot{\epsilon}_{SS} \quad (9)$$

After integrating $\dot{\epsilon}$, it is possible determine the total creep strain (ϵ) as:

$$\epsilon(t) = \int_0^t (F \dot{\epsilon}_{SS}) dt \quad (10)$$

2.1 Validation

The Multiple Deformation Mechanism model is very effective to simulate the salt rock behavior. Munson (1979) presents accurate results for simulations involving experimental and field situations. Thus, this paper does not prove the model efficiency, which is very used and established. The purpose of validation is to verify that the model implementation using the Fortran language was performed correctly. This implementation is necessary as this model is not native to the software.

Three triaxial creep tests was simulated to validate the implementation. During the validation simulation the samples was kept under confining stress of 10 MPa and deviatoric stress of 10, 14, and 17 MPa. Poiate Junior et al. (2006) presented the test with deviatoric stress of 10 MPa, while Costa et al. (2005) presented the other tests.

All tests simulated was performed using cylindrical body tests of 88.9 mm (3.5 inches) diameter and 177.8 mm (7.0 inches) length. The aspect ratio of 2 for 1 follows the recommendation of the International Society for Rock Mechanics. During the test, the temperature was controlled and kept at 86 °C.

Figure 1 presents both experimental and numerical results obtained for the samples. Table 1 presents the parameters used

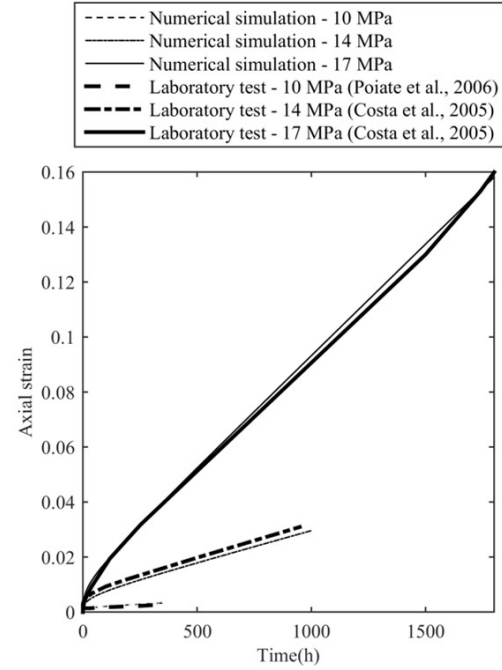


Figure 1. Comparison between numerical results and experimental results of triaxial tests on halite.

Table 1. Parameters used to characterize the creep behavior of the rock salt.

Parameter	Unit	Value
A_1	s^{-1}	1.638×10^{27}
Q_1	kJ/mol	1.045×10^5
n_1	-	7.2
B_1	s^{-1}	9.981×10^6
A_2	s^{-1}	1.924×10^6
Q_2	kJ/mol	4.18×10^4
n_2	-	3.2
B_2	s^{-1}	4.976×10^{-2}
σ_0	MPa	20.57
q	-	9.335×10^3
R	$J (mol.K)^{-1}$	8.3143
m	-	3.0
K_0	-	7.750×10^4
c	K^{-1}	0.009198
α	-	-17.37
θ	-	-7.738
δ	-	0.58

to perform the numerical simulations. Firme et al. (2016). calibrated the parameters using tests of Sergipe-Alagoas-Brazil basin. Adequated agreement was observed between numerical and experimental results.

To characterize the elastic phase of the material was adopted the values presented by Poiate Junior (2012).

The author used 20.4 GPa and $21.29 \text{ kN} / \text{m}^3$ to describe the Halite's dynamic elastic modulus, and unit specific weight. Finally, we used the dynamic Poisson's ratio equal to 0.36 as presented by Costa et al. (2005).

3. Stratigraphy and typical geometry

The geometries of chlorine-soda mines are very variable due to their construction techniques and the material characteristics. The cavern studied in this paper has geometry and dimensions similar to existing mines in northeastern Brazil (CPRM, 2019). Figure 2 shows the geometry of the mine studied and its dimensions obtained by sonar measurement.

The stratigraphy used is based on the characteristics of the Sergipe-Alagoas sedimentary basin, also located in northeastern Brazil. In this basement, the rock salt stratum starts at approximately 900 m of depth and the overburden is composed mainly of shale and sandstone, and there may be the presence of other sedimentary rocks.

In this paper, it was considered the most recent geometry obtained by sonar measurement performed in 2018. However, the geometry was simplified by replacing the original format by an ellipse, with height and radius similar to the original geometry. Figure 3 shows the simplified geometry.

The simulation, despite being based on data of parameters and geometry of Brazilian mines, is not representative of any specific case, it is a hypothetical situation that aims to analyze the behavior for conditions similar to that simulated.

Simplifications are common in studies of underground salt caverns (Goulart et al., 2020; Li et al., 2021). They bring the advantage of avoiding the action of stress concentrators due to the corners. Another important point is the quality of the mesh used to discretize the model. A simpler geometry avoids the use of a greater number of elements in regions with sharp corners, for example. Furthermore, discretization can be performed with more robust elements. This provides an improvement in determining the variables involved in the simulation.

4. Geomechanical model, boundary, and initial conditions

Figure 3 presents the model used for performing the simulations. At the top of the model was applied a 19.03 MPa pressure, which characterizes the overburden. This pressure represents the sediments above the shale layer. The height of the mine is 96 m and the approximate radius is 55 m . Figure 3 also presents the others measurements of the model.

The finite element model was built using the commercial software Abaqus. An axisymmetric model represented the saline environment. It was used CAX4R elements (4-node bilinear axisymmetric quadrilateral, reduced integration) to discretize the model.

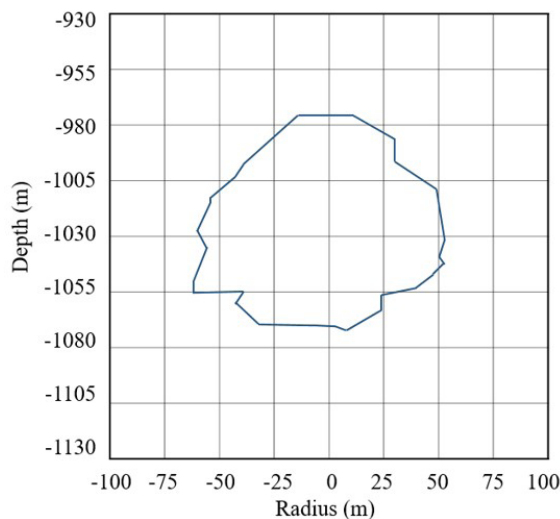


Figure 2. Shape and dimensions of cavern obtained by the sonar survey in 2018 (CPRM, 2019).

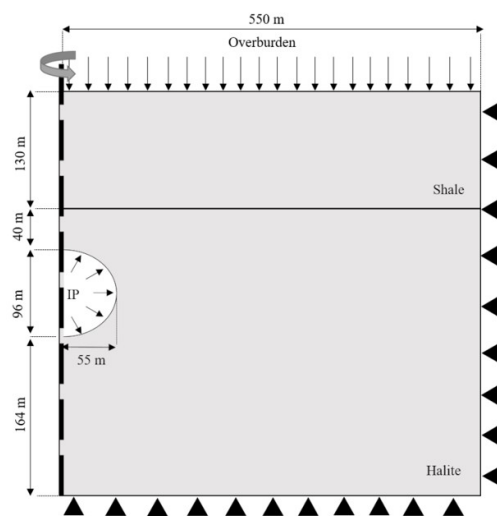


Figure 3. Geometry used for representing the cavern.

Two materials composed the model: halite and shale (Figure 3). We applied the elastoplastic model proposed by Mohr-Coulomb to the shale's behavior. It was considered the elastic modulus, Poisson's ratio, friction angle, cohesion and the specific weight equal to 18.97 GPa , 0.15 , 22° , 4.8 MPa and 24.00 kN/m^3 (Costa et al., 2015). The geothermal gradients, i.e., the temperature rate of geotechnical materials, suggested by Costa et al. (2012) were used. The temperature is higher the greater the depth, these authors suggest 10°C/km for saline material and 30°C/km for the sedimentary rocks that constitute the overburden.

Figure 4a presents the mesh discretization around the cavern and the five points of interest (A, B, C, D, e E). These points were used to perform some analysis presented in

section 4. Figure 4b presents the mesh and boundary conditions. The thick black line indicates the mesh axis of revolution to build the model. Figure 4b represents a 90-degree revolution of Figure 3. However, the software understands the model as a complete 360-degree revolution. The blue and gray portions represent shale and halite.

On the right side, the horizontal displacement was constrained. This restriction represents the continuity of the layer and allows the vertical movement. Vertical displacements were constrained at the model bottom.

The simulation was performed in three steps. In the first step, the geostatic stresses are generated, and the excavation of the mine is carried out. The coefficient of earth pressure at rest of overburden was considered 0.25 and for salt rock was considered 1, cause your creep behavior. The excavation is carried out instantly with the complete removal of the material. The second step is the instantaneous elastic behavior of the material. Finally, the third step is visco-elasto-plastic behavior using the Multiple Deformation Mechanism model concerning a period of 50 years.

Given the fact that some units of the constitutive model use seconds as a time unit, the simulations were performed considering seconds as the time unit. The time for data processing of each simulation is directly linked to the internal pressure considered. Higher internal pressures are more stable conditions. So, they are more agile, while smaller internal pressures need more time to be completed. The simulations performed in this research took between 10 and 30 minutes using an Intel Core I7 computer with 8GB of RAM.

5. Numerical experiments and stability criteria

Five simulations were performed by considering different internal pressures applied on the cavern (Table 2). The values of the internal pressures are a percentage of the effective vertical tension at the top of the cavern. Those values ranging from 40% to 80% of the value of the effective vertical tension.

The analyzed internal pressures were based on literature to choose, which indicates values between 30% and 85% of the effective vertical stress at the top of the cavern. Pressures less than 30% cause instability in the caverns. While pressures greater than 85% can generate tensile stress. Salt rocks do not resist this type of effort (Bérest et al., 2020; Costa et al., 2015; Yuan et al., 2021). Stability criteria considered both the creep and dilatation behaviors.

5.1 Creep criterion

The creep behavior causes a decrease in the volume of salt caverns. Thus, the creep criterion relates to the cavern volume loss. The largest shrinkage volume limit was defined as 10% of the initial cavern volume throughout the analysis

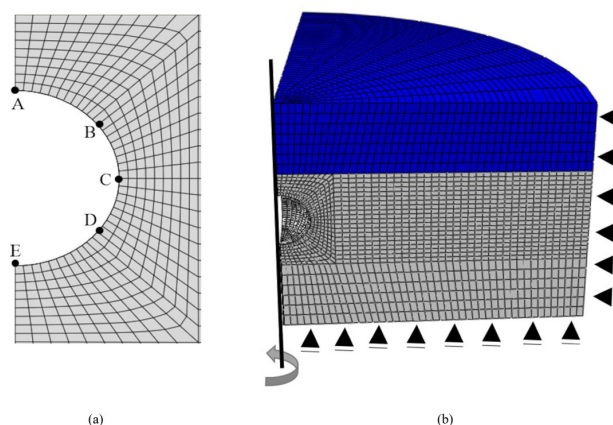


Figure 4. Axisymmetric model and finite element mesh discretization: (a) detail of the analysis points; (b) partial revolution of the analysis plane.

Table 2. Design of experiments.

Internal pressure (MPa)	Symbol
9.19	IP40
11.49	IP50
13.79	IP60
16.09	IP70
18.38	IP80

(50 years). This is a value often used in salt cavern stability analyses (Yuan et al., 2021).

5.2 Dilatancy criterion

In this research, the tertiary (accelerated) stage of creep was not considered. However, an expansion criterion monitored the damage in the salt rock. Salt rocks in situ are usually impermeable. But, when an increase in deformation happens, there is a rise in permeability of the rock due to damage (Van Sambeek et al., 1993; Firme et al., 2016). Ratigan's criterion (Van Sambeek et al., 1993) was used, since this criterion is widely used to model the Brazilian halite (Costa et al., 2015; Firme et al., 2016; Firme et al., 2019). This criterion considers the mean stress (σ_m) of each point to estimate a critical deviatoric stress ($\sigma_{d,cr}$) for that point by following equation:

$$\sigma_{d,cr} = (a\sigma_m)\sqrt{3} \quad (11)$$

in which a receives the value of 0.81.

Damage will occur if the ratio between the deviatoric (σ_d) effective stress and the critical deviatoric stress ($\sigma_{d,cr}$) is greater than the critical value indicated by the criterion. This value corresponds to 0.8, i.e., the ratio between the acting deviatoric effective stress and critical deviatoric stress is the micro-crack ratio (MC) defined as:

$$MC = \frac{\sigma_d}{\sigma_{d,cr}} \quad (12)$$

The deviatoric effective stress (σ_d) considered in this paper is the equivalent von Mises stress ($\sigma_d = \sqrt{3J_2}$) that can be described from the second invariant of the deviatoric stress tensors (J_2).

6. Results

6.1 Salt cavern convergence

As highlighted above, the creep behavior is responsible for the convergence of salt caverns. That is, the volume of shrinkage of the cavern. The strain at each point of the model depends on the acting deviatoric stress (von Mises equivalent stress), as shown in Equations 1, 2, and 3. Thus, the shrinkage volume is dependent on the von Mises equivalent stress.

The Figure 5 shows the von Mises equivalent stress for IP40. One can observe that the cap rock causes a stress arching effect. This relieves the stresses in the saline material. Thus, cap rock is very important for cavern simulations. Zhang et al. (2020a) also verified the importance of the surrounding rocks.

Figure 6 shows the equivalent creep strains for all internal pressures presented in Table 2. The point C was presented the highest level of strain among five points.

Figure 7 shows the wall equivalent strain rate at point C for all analyzed internal pressures. It was analyzed this point because it is at the region with the highest strain. Costa et al. (2015) indicates an admissible creep rate in steady-state regime equal to 0.5×10^{-06} per hour. One can note that the strain rates (per hour) are between 10^{-07} and 10^{-10} at the end of analysis. Instantly the creep strain rate has values greater than the admissible value for all internal pressures. However, in a small portion of time, the creep rate becomes higher than the admissible value. Afterwards, one can observe the deceleration

phase of the strain rate until reaching the steady-state. There is an unstable condition for the IP80. However, the creep rate presents the smallest values at the end of simulation.

Figure 8 shows the wall equivalent strain at point C. In the numerical analysis performed, the maximum strain was 0.038 for IP40. The simulations did not reach the maximum value allowable considered equal to 0.100 (Costa et al., 2015). This indicates that shrinkage caused by salt creep is not meaningful even for IP40, which presents an increasing behavior during the simulation.

Figure 9 shows the percentage of volume shrinkage over time. None of the numerical experiments reached the maximum shrinkage volume of 10% of the initial volume.

Figure 10 presents the numerical results of displacements norm resulting from creep strain. Clearly, displacements decreased when the internal pressure increases.

A large displacement increase was noted when the internal pressure was reduced from 80% to 70% of the in situ vertical stress on the mine roof. Bérest et al. (2020) performed several studies on the internal pressure of salt caverns. They indicate that the adequate pressure is between 80 and 85% of the in situ vertical stress on the mine roof. However, it is not always possible to ensure this pressurization, due to several factors such as reactivation of geological faults, cracks due to the low tensile strength of the saline material or, even, due to leakage due to the filling of the well.

6.2 Dilatant behavior

Figure 11 presents the micro-cracking (MC) ratio obtained for each internal pressure considered. One observes that the regions close to points B and C provide the necessary condition for initiation the micro cracks.

At the end of the 50 years analyzed by finite element modeling, the micro-crack ratio was acceptable only for IP70 and IP80. Figure 12 shows the micro-cracking ratio values, considering 50 years of analysis, for point C for all simulated internal pressures.

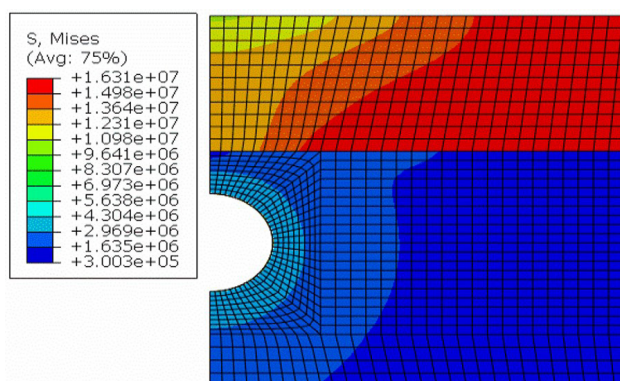


Figure 5. Von Mises equivalent stress regarding the IP40.

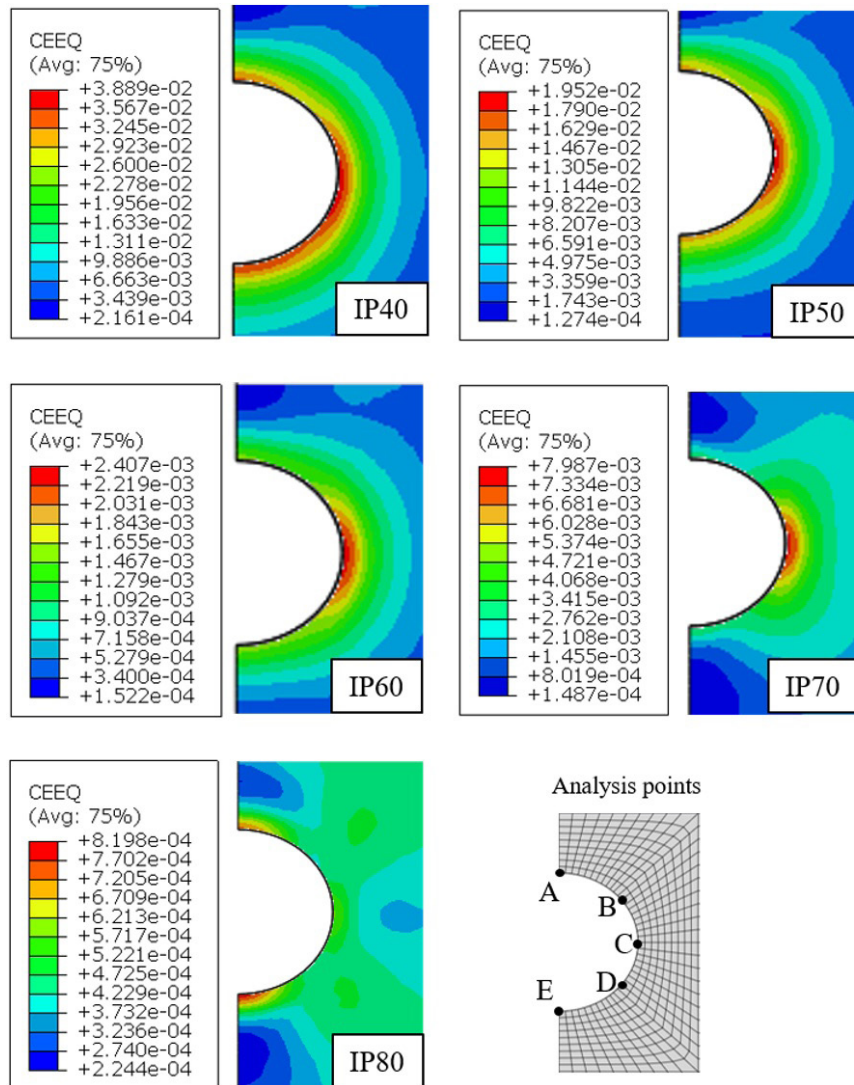


Figure 6. Equivalent creep strains (CEEQ) around the cavern for the internal pressures studied.

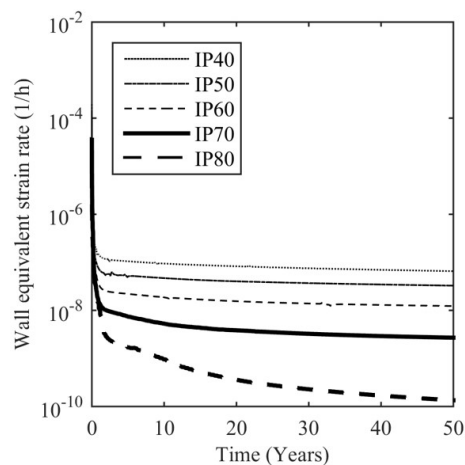


Figure 7. Wall equivalent strain rate at point C.

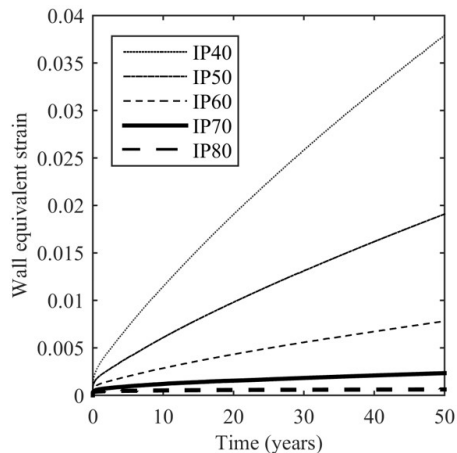


Figure 8. Wall equivalent strain at point C.

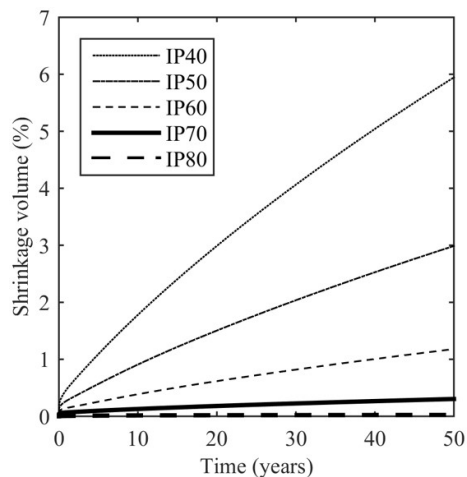


Figure 9. Percentage of volume shrinkage over time.

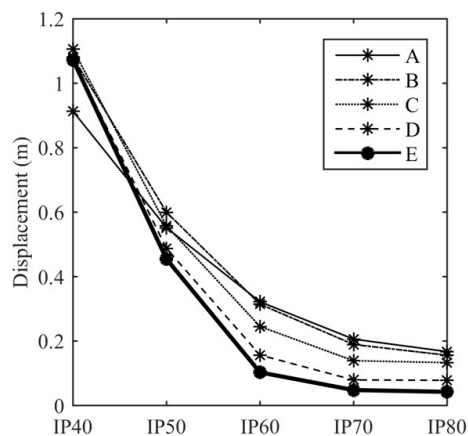


Figure 10. Magnitude of displacements at the analyzed points.

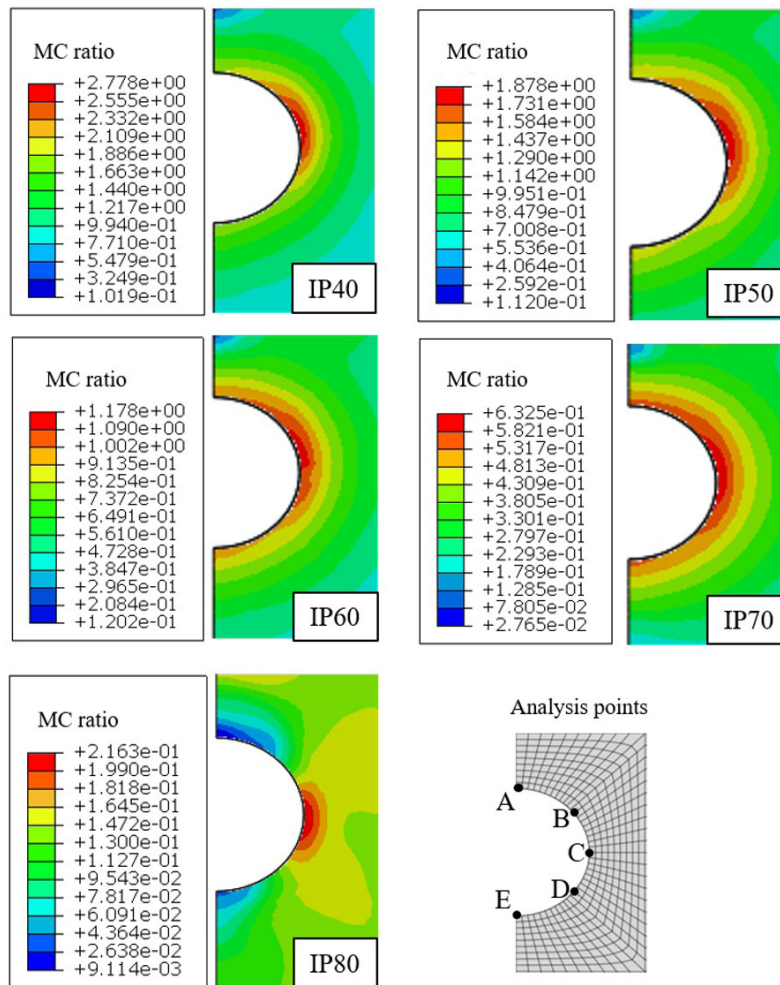


Figure 11. Micro-cracking ratio (MC) around the cavern for the internal pressures studied.

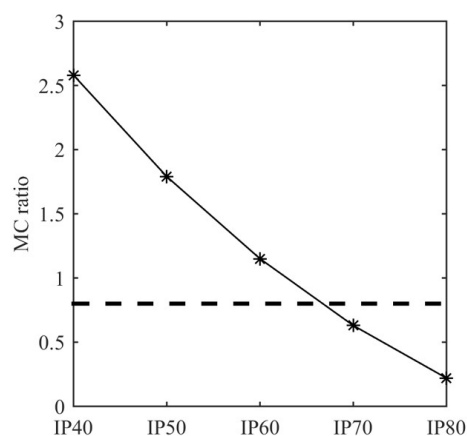


Figure 12. MC ratio at point C after 50 years of analysis. Dashed line represents the dilatancy criterion critical value.

7. Conclusions

The high level of stress due to the creep phenomenon in salt rocks can cause the failure of abandoned caverns.

In this sense, the knowledge of this complex behavior is fundamental. The use of Multiple Deformation Mechanism model combined with a suitable dilatation criterion allows modeling the primary creep, the steady-state creep and damage

of a salt cavern. Thus, one can perform numerical studies by considering the modifications of the cavern's geometry or the internal pressure.

Simulations were carried out, using the finite element method, to analyze the behavior of caverns located in saline environments. Creep and dilation were investigated. Despite the occurrence of displacements with high magnitude (greater than 1 m), the creep deformation for all analyzed internal pressure was considered acceptable, as the shrinkage volume was smaller than the maximum allowable shrinkage volume. Another important aspect simulated was the micro-crack ratio. It was considered as an acceptable value of 0.8. Values greater than this indicate the occurrence of micro-cracks in the cavern walls. This paper indicates that only the IP70 and IP80 condition provided acceptable results.

Several researches have been carried out in order to analyze the behavior of salt-rock caverns, but there are difficulties in representing the behavior of this material over time. It is necessary to emphasize that the combination of a model that simulates primary and secondary creep with a damage criterion, as done in this research, is one of the most robust ways of analyzing rock salt behavior over time. Finally, the integrated analysis between creep and dilatant behavior was considered an important tool for reliability analysis, as it allows an accurate analysis of the behavior of rock salts. Future research should focus on analyzing the variability of geotechnical parameters to also provide a probabilistic approach.

Acknowledgements

The authors are grateful to the Post-Degree in Civil Construction Engineering from Federal University of Paraná (PPGECC-UFPR) and to the Araucária Foundation for enabling such a study. This work was carried out with the support of Coordination of Improvement of Personnel of Higher Education - Brazil (CAPES) - Code of Financing 001. J. T. Pereira acknowledges the financial support from National Council for Scientific and Technological Development (CNPq/Brazil).

Declaration of interest

The authors have no conflicts of interest to declare. All co-authors have observed and affirmed the contents of the paper and there is no financial interest to report.

Authors' contributions

Renathelly Fernanda da Silva Brunetta: conceptualization, data curation, visualization, writing – original draft. Alessandro C. M. Kormann: formal analysis, funding acquisition, investigation, methodology, project administration, resources, software. José Eduardo Gubaua: conceptualization, data

curation, methodology, supervision, validation, writing – original draft. Jucélio Tomás Pereira: supervision, validation, writing – review & editing.

Data availability

The datasets generated and analyzed during the current study are available from the corresponding author upon request.

List of symbols

c	theoretical material's constants
m	theoretical material's constants
n_1	stress power of the Dislocation Climb Mechanism
n_2	stress power of the undefined mechanism
q	stress parameter
A_1	structure factor of the Dislocation Climb Mechanism
A_2	structure factor of the undefined mechanism
B_1	structure factor of the Dislocation Glide Mechanism
B_2	structure factor of the Dislocation Glide Mechanism
G	elastic shear modulus
H	heaviside step function
K_0	transient parameter
Q_1	thermal activation energy of the Dislocation Climb Mechanism
Q_2	thermal activation energy of the undefined mechanism
R	universal gas constant
T	temperature
α_h	internal isotropic hardening variable
α_s	internal isotropic softening variable
β_h	internal isotropic hardening variable
β_s	internal isotropic softening variable
Δ	hardening parameter
δ	softening parameter
$\dot{\epsilon}_{DC}$	Dislocation Climb strain rate
$\dot{\epsilon}_{DG}$	Dislocation Glide strain rate
$\dot{\epsilon}_{SS}^*$	steady-state strain rate
ϵ_t^*	limit strain during the transient creep
$\dot{\epsilon}_{UM}$	undefined mechanism strain rate
σ_0	reference stress value of the mechanism
σ_{eq}	von Mises equivalent stress

References

- Autin, W.J. (2002). Landscape evolution of the Five Islands of south Louisiana: scientific policy and salt dome utilization and management. *Geomorphology*, 47, 227-244. [http://dx.doi.org/10.1016/S0169-555X\(02\)00086-7](http://dx.doi.org/10.1016/S0169-555X(02)00086-7).
- Bell, F.G., Stacey, T.R., & Genske, D.D. (2000). Mining subsidence and its effect in the environment: some differing examples. *Environmental Geology*, 40, 135-152. <http://dx.doi.org/10.1007/s002540000140>.
- Bérest, P., Brouard, B., Karimi-Jafari, M., & Réveillère, A. (2020). Maximum admissible pressure in salt caverns

- used for brine production and hydrocarbon storage. *Oil & Gas Science and Technology*, 75, 1-15. <http://dx.doi.org/10.2516/ogst/2020068>.
- Costa, A.M. (1984). *An application of computational methods and rock mechanics principles in the design and analysis of mining excavations* [Doctoral thesis, Pontifical Catholic University of Rio de Janeiro]. Pontifical Catholic University of Rio de Janeiro's repository (in Portuguese).
- Costa, A.M., Amaral, C.S., & Poiate Junior, E. (2015). Hydrocarbon production and storage using offshore underground salt caverns. In L. Roberts, K. Mellegard & F. Hansen (Eds.), *Mechanical behaviour of salt VIII* (pp. 211-220). Boca Raton: CRC Press. <https://doi.org/10.1201/b18393-28>.
- Costa, A.M., Amaral, C.S., Poiate Junior, E., Pereira, A.M.B., Martha, L.F., Gattass, M., & Roehl, D. (October 16-21, 2012). Underground storage of natural gas and CO₂ in salt caverns in deep and ultra-deep water offshore Brazil. In Q. Qian & Y. Zhou (Eds.), *Proceedings of the 12th ISRM International Congress on Rock Mechanics* (pp. 1659-1664). Boca Raton, USA: CRC Press.
- Costa, A.M., Poiate Junior, E., Falcão, J.L., & Coelho, L.F.M. (February 23-25, 2005). Triaxial creep tests in salt applied in drilling through thick salt layers in campos Basin-Brazil. In *SPE/IADC Drill Conference* (pp. 1009-1017). Red Hook, USA: Curran Associates, Inc. <https://doi.org/10.2523/92629-MS>.
- CPRM. (2019). *Estudo sobre a instabilidade do terreno nos bairros Pinheiro, Mutange e Bebedouro, Maceió (AL). Geofísica – gravimetria* (Vol. II). Brasília: CPRM. Retrieved in June 23, 2022, from https://rigeo.cprm.gov.br/jspui/bitstream/doc/21134/9/volumeII_j.pdf (in Portuguese).
- Crotogino, F., & Kepplinger, J. (2006). *Cavern well abandonment techniques guidelines manual*. Hannover: SMRI.
- Curi, A. (2017). *Lavra de minas*. São Paulo: Oficina de Textos (in Portuguese).
- Firme, P.A.L.P., Roehl, D., & Romanel, C. (2016). An assessment of the creep behaviour of Brazilian salt rocks using the multi-mechanism deformation model. *Acta Geotechnica*, 11, 1445-1463. <http://dx.doi.org/10.1007/s11440-016-0451-y>.
- Firme, P.A.L.P., Roehl, D., & Romanel, C. (2019). Salt caverns history and geomechanics towards future natural gas strategic storage in Brazil. *Journal of Natural Gas Science and Engineering*, 72, 103006. <http://dx.doi.org/10.1016/j.jngse.2019.103006>.
- Goulart, M.B.R., Costa, P.V.M., Costa, A.M., Miranda, A.C.O., Mendes, A.B., & Ebecken, N.F.F. (2020). Technology readiness assessment of ultra-deep Salt caverns for carbon capture and storage in Brazil. *International Journal of Greenhouse Gas Control*, 99, 103083. <http://dx.doi.org/10.1016/j.ijggc.2020.103083>.
- Jörissen, J. (2014). Chlorine and caustic technology, overview and traditional processes. In G. Kreysa, K.-I. Ota & R. F. Savinell (Eds.), *Encyclopedia of applied electrochemistry* (pp. 194-200). New York: Springer. https://doi.org/10.1007/978-1-4419-6996-5_297.
- Li, P., Li, Y., Shi, X., Zhao, K., Liu, X., & Ma, H. (2021). Prediction method for calculating the porosity of insoluble sediments for salt cavern gas storage applications. *Energy*, 221, 119815. <http://dx.doi.org/10.1016/j.energy.2021.119815>.
- Munson, D.E. (1979). *Preliminary deformation-mechanism map for salt (with application to WIPP)*. Albuquerque: Sandia Laboratories. Report n° SAND-79-0076. <https://doi.org/10.2172/6499296>.
- Munson, D.E., & Dawson, P.R. (1979). *Constitutive model for the low temperature creep of salt (with application to WIPP)*. Albuquerque: Sandia Laboratories. Report n° SAND-79-1853. <https://doi.org/10.2172/5729479>.
- Poiate Junior, E. (2012). *Rock mechanics and computational mechanics for the design of oil wells in salt zones* [Doctoral thesis, Pontifical Catholic University of Rio de Janeiro]. Pontifical Catholic University of Rio de Janeiro's repository (in Portuguese). <https://doi.org/10.17771/PUCRio.acad.34904>.
- Poiate Junior, E., Costa, A.M., & Falcao, J.L. (February 21-23, 2006). Well design for drilling through thick evaporite layers in Santos Basin - Brazil. In *SPE/IADC Drill Conference* (pp. 1081-1096). Red Hook, USA: Curran Associates, Inc. <https://doi.org/10.2523/99161-ms>.
- Thoraval, A., Lahaie, F., Brouard, B., & Berest, P. (2015). A generic model for predicting long-term behavior of storage salt caverns after their abandonment as an aid to risk assessment. *International Journal of Rock Mechanics and Mining Sciences*, 77, 44-59. <http://dx.doi.org/10.1016/j.ijrmms.2014.10.014>.
- Van Sambeek, L.L., Ratigan, J.L., & Hansen, F.D. (1993). Dilatancy of rock salt in laboratory tests. *International Journal of Rock Mechanics and Mining Sciences*, 30, 735-738. [http://dx.doi.org/10.1016/0148-9062\(93\)90015-6](http://dx.doi.org/10.1016/0148-9062(93)90015-6).
- Vassileva, M., Al-Halbouni, D., Motagh, M., Walter, T.R., Dahm, T., & Wetzel, H.U. (2021). A decade-long silent ground subsidence hazard culminating in a metropolitan disaster in Maceió, Brazil. *Scientific Reports*, 11, 7704. <https://doi.org/10.1038/s41598-021-87033-0>.
- Wang, T., Yang, C., Chen, J., & Daemen, J.J.K. (2018). Geomechanical investigation of roof failure of China's first gas storage salt cavern. *Engineering Geology*, 243, 59-69. <http://dx.doi.org/10.1016/j.enggeo.2018.06.013>.
- Wei, L., Jie, C., Deyi, J., Xilin, S., Yinping, L., & Daemen, J.J.K. (2016a). Tightness and suitability evaluation of abandoned salt caverns served as hydrocarbon energies storage under adverse geological conditions (AGC). *Applied Energy*, 178, 703-720. <https://doi.org/10.1016/j.apenergy.2016.06.086>.
- Wei, L., Yinping, L., Chunhe, Y., Deyi, J., Daemen, J.J.K., & Jie, C. (2016b). A new method of surface subsidence prediction for natural gas storage cavern in bedded rock salts. *Environmental Earth Sciences*, 75, 800. <http://dx.doi.org/10.1007/s12665-016-5611-8>.

- Whyatt, J., & Varley, F. (July 29-31, 2008). Catastrophic failures of underground evaporite mines. In S. S. Peng, C. Mark, G. L. Finfinger, S. C. Tadolini, A. W. Khair, K. A. Heasley & Y. Luo (Eds.), *27th International Conference on Ground Control Mining* (pp. 113-122). Morgantown, USA: West Virginia University.
- Yerro, A., Corominas, J., Monells, D., & Mallorquí, J.J. (2014). Analysis of the evolution of ground movements in a low densely urban area by means of DInSAR technique. *Engineering Geology*, 170(20), 52-65. <https://doi.org/10.1016/j.enggeo.12.002>.
- Yuan, G., Wan, J., Li, J., Li, G., Xia, Y., & Ban, F. (2021). Stability analysis of a typical two-well-horizontal saddle-shaped salt cavern. *Journal of Energy Storage*, 40, 102763. <http://dx.doi.org/10.1016/j.est.2021.102763>.
- Zhang, G., Wang, Z., Liu, J., Li, Y., Cui, Z., Zhang, H., Wang, L., & Sui, L. (2020a). Stability of the bedded key roof above abandoned horizontal salt cavern used for underground gas storage. *Bulletin of Engineering Geology and the Environment*, 79, 4205-4219. <http://dx.doi.org/10.1007/s10064-020-01830-x>.
- Zhang, N., Shi, X., Zhang, Y., & Shan, P. (2020b). Tightness analysis of underground natural gas and oil storage caverns with limit pillar widths in bedded rock salt. *IEEE Access*, 8, 12130-12145. <http://dx.doi.org/10.1109/ACCESS.2020.2966006>.